Chapter II.3
Square-Wave Voltammetry

Milivoj Lovrić

II.3.1 Introduction

Square-wave voltammetry (SWV) is one of the four major voltammetric techniques provided by modern computer-controlled electroanalytical instruments, such as Autolab and μAutolab (both EcoChemie, Utrecht), BAS 100 A (Bioanalytical Systems), and PAR Model 384 B (Princeton Applied Research) [1]. The other three important techniques are single scan and cyclic staircase, pulse, and differential pulse voltammetry (see Chap. II.2). All four are either directly applied or after a preconcentration to record the stripping process. The application of SWV boomed in the last decade, first because of the widespread use of the instruments mentioned above, second because of a well-developed theory, and finally, and most importantly, because of its high sensitivity to surface-confined electrode reactions. Adsorptive stripping SWV is the best electroanalytical method for the determination of electroactive organic molecules that are adsorbed on the electrode surface [2].

The theory and application of SWV are described in several reviews [2–7], and here only a brief account of the recent developments will be given. Contemporary SWV originates from the Kalousek commutator [8] and Barker's square-wave polarography [9, 10]. The Kalousek commutator switched the potential between a slowly varying ramp and a certain constant value to study the reversibility of electrode reactions [11–13]. Barker employed a low-amplitude symmetrical square wave superimposed on a ramp and recorded the difference in currents measured at the ends of two successive half-cycles, with the objective to discriminate the capacitive current [14–16]. SWV was developed by combining the high-amplitude, high-frequency square wave with the fast staircase waveform and by using computer-controlled instruments instead of analog hardware [17–26]. Figure II.3.1 shows the potential–time waveform of modern SWV. Each square-wave period occurs during one staircase period τ. Hence, the frequency of excitation signal is $f = \tau^{-1}$, and the pulse duration is $t_p = \tau/2$. The square-wave amplitude,

M. Lovrić (✉)
Rudjer Boskovic Institute, 10001 Zagreb, Croatia
e-mail: mlovric@irb.hr

F. Scholz (ed.), *Electroanalytical Methods*, 2nd ed.,
DOI 10.1007/978-3-642-02915-8_6,

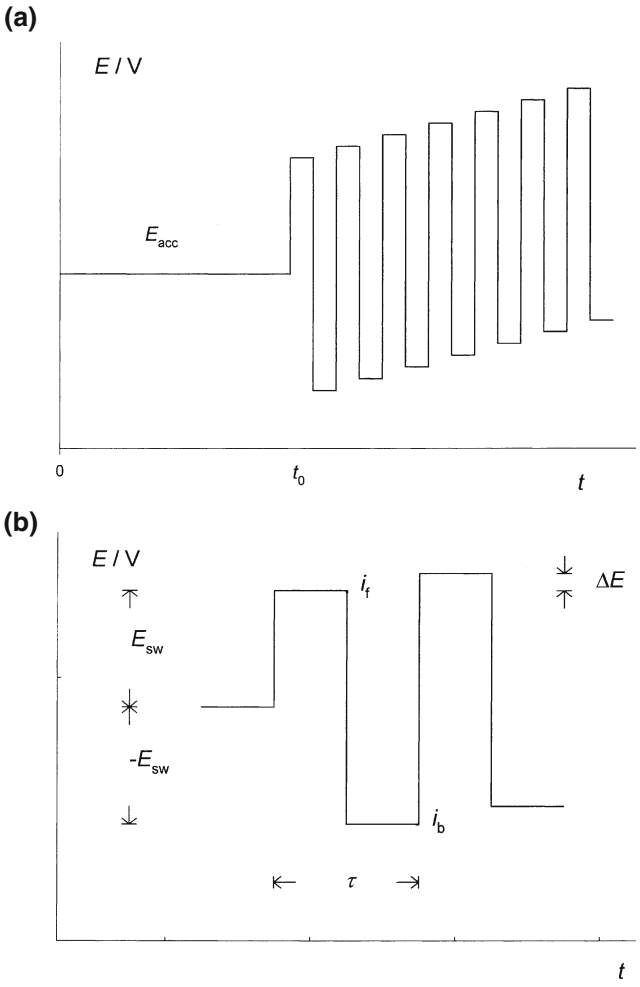

Fig. II.3.1 Scheme of the square-wave excitation signal. E_{acc} starting potential; t_0 delay time; E_{sw} SW amplitude; ΔE scan increment; τ SW period; i_f forward current; i_b backward current, and (•) points where they were sampled

E_{sw}, is one-half of the peak-to-peak amplitude, and the potential increment ΔE is the step height of the staircase waveform. The scan rate is defined as $\Delta E/\tau$. Relative to the scan direction, ΔE, forward and backward pulses can be distinguished. The currents are measured at the end of each pulse and the difference between the currents measured on two successive pulses is recorded as a net response. Additionally, the two components of the net response, i.e., the currents of the forward and backward series of pulses, respectively, can be displayed as well [6, 27–30]. The currents are plotted as a function of the corresponding potential of the staircase waveform.

II.3.2 Simple Reactions on Stationary Planar Electrodes

Figure II.3.2 shows the dimensionless square-wave net response $\Delta\Phi = \Delta i[nFSc^*(D_\mathrm{r}f)^{1/2}]^{-1}$ of a simple, fast, and reversible electrode reaction

$$\mathrm{Red} \rightleftarrows \mathrm{Ox} + n\mathrm{e}^- \tag{II.3.1}$$

where n is the number of electrons, F is the Faraday constant, S is the surface area of the electrode, c^* is the bulk concentration of the species Red, D_r is the diffusion coefficient of the species Red, f is the square-wave frequency and $E_{1/2}$ is the half-wave potential of the reaction (Eq. II.3.1). The response was calculated by using the planar diffusion model (see the Appendix, Eqs. II.3.24 and II.3.30). The dimensionless forward Φ_f and backward Φ_b components of the response are also shown in Fig. II.3.2. The net response ($\Delta\Phi = \Phi_\mathrm{f} - \Phi_\mathrm{b}$) and its components Φ_f and Φ_b consist of discrete current-staircase potential points separated by the potential increment ΔE [6, 17–19]. For a better graphical presentation, the points can be interconnected, as in Fig. II.3.2, but the line between two points has no physical significance. Hence, ΔE determines the density of information in the SWV response. However, the response depends on the product of the number of electrons and the potential increment (for the meaning of dimensionless potential φ_m^*, see Eqs. II.3.26 and II.3.30): $\varphi_\mathrm{m}^* = F(nE_m - nE_{1/2})/RT$, and $nE_\mathrm{m} = nE_\mathrm{st} + nE_\mathrm{sw}(1 \le m \le 25), nE_m =$

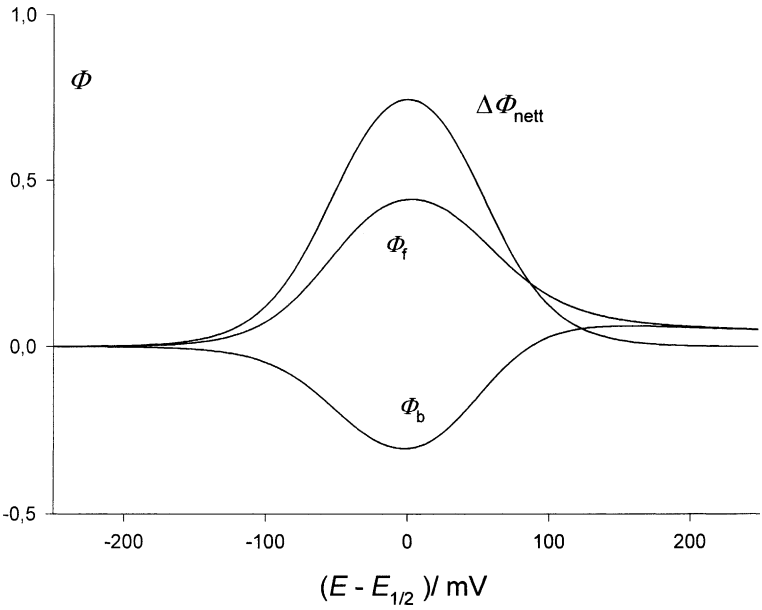

Fig. II.3.2 Square-wave voltammogram of fast and reversible redox reaction (II.3.1). $nE_\mathrm{sw} = 50\,\mathrm{mV}$ and $n\Delta E = 2$ mV. The net response ($\Delta\Phi_\mathrm{nett}$) and its forward (Φ_f) and backward (Φ_b) components

$nE_{st} - nE_{sw}(26 \leq m \leq 50), nE_m = nE_{st} + nE_{sw} + n\Delta E(51 \leq m \leq 75), nE_m = nE_{st} - nE_{sw} + n\Delta E(76 \leq m \leq 100)$, etc. Besides, $E_{stair} = E_{st}(1 \leq m \leq 50)$ and $E_{stair} = E_{st} + \Delta E(51 \leq m \leq 100)$, etc. The larger the product $n\Delta E$, the larger will be the net response $\Delta\Phi$. This is because the experiment is performed on a solid electrode, or a single mercury drop, and the apparent scan rate is linearly proportional to the potential increment: $v = f\Delta E$. So, the response increases if the density of information is diminished (for the same frequency). Regardless of ΔE, there is always a particular value of $\Delta\Phi$ that is the highest of all. This is the peak current $\Delta\Phi_p$, and the corresponding staircase potential is the peak potential E_p. The latter is measured with the precision ΔE. In essence, there is no theoretical reason to interpolate any mathematical function between the two experimentally determined current–potential points. If ΔE is smaller, all $\Delta\Phi$ points, including $\Delta\Phi_p$, are smaller too. Frequently, the response is distorted by electronic noise and a smoothing procedure is necessary for its correct interpretation. In this case it is better if ΔE is as small as possible. By smoothing, the set of discrete points is transformed into a continuous current–potential curve, and the peak current and peak potential values can be affected slightly.

The dimensionless net peak current $\Delta\Phi_p$ primarily depends on the product nE_{sw} [31]. This is shown in Table II.3.1. With increasing nE_{sw} the slope $\partial\Delta\Phi_p/\partial nE_{sw}$ continuously decreases, while the half-peak width increases. The maximum ratio between $\Delta\Phi_p$ and the half-peak width appears for $nE_w = 50\,\text{mV}$ [6]. This is the optimum amplitude for analytical measurements. If $E_{sw} = 0$, the square-wave signal turns into the signal of differential staircase voltammetry, and $\Delta\Phi_p$ does not vanish [6, 32, 33].

The peak currents and potentials of the forward and backward components are listed in Table II.3.2. If the square-wave amplitude is not too small ($nE_{sw} > 10\,\text{mV}$), the backward component indicates the reversibility of the electrode reaction. In the

Table II.3.1 Dimensionless net peak currents of square-wave voltammograms of fast and reversible redox reaction (II.3.1)

$\Delta\Phi_p$			
nE_{sw}	$n\Delta E$/mV		
mV	2	4	6
0	0.0084	0.0160	0.0230
5	0.1043	0.1116	0.1183
10	0.1984	0.2053	0.2118
20	0.3744	0.3805	0.3863
30	0.5265	0.5316	0.5367
40	0.6505	0.6546	0.6588
50	0.7467	0.7499	0.7533
60	0.8186	0.8210	0.8237
70	0.8707	0.8726	0.8747
80	0.9077	0.9092	0.9108
90	0.9337	0.9348	0.9361
100	0.9517	0.9525	0.9535

case of reaction (II.3.1), this means that the reduction of the product Ox occurs. If $nE_{sw} < 10\,mV$, there is no minimum of the backward component. For the optimum amplitude, the separation of peak potentials of two components is 4 mV. The separation vanishes if $nE_{sw} = 70\,mV$, but increases to 18 mV if $nE_{sw} = 20\,mV$. At these amplitudes the peak potential of the anodic component is higher than the potential of the cathodic component, but, if $nE_{sw} \geq 80\,mV$, these potentials are inverted, as can be seen in Table II.3.2. The peak potentials of both components as well as of the net response are independent of the square-wave frequency, and this is the best criterion of the reversibility of reaction (II.3.1) [34, 35].

The net peak current depends linearly on the square root of the frequency:

$$\Delta i_p = nFSD_r^{1/2}\Delta\Phi_p f^{1/2} c^* \qquad \text{(II.3.2)}$$

(where $\Delta\Phi_p$ depends on nE_{sw} and $n\Delta E$). The condition is that the instantaneous current is sampled only once at the end of each pulse, but then the response may appear noisy [36]. This procedure was assumed in the theoretical calculations presented in Fig. II.3.2 and Tables II.3.1 and II.3.2. In general, several instantaneous currents can be sampled at certain intervals during the last third, or some other portion of the pulse, and then averaged [1]. The average response corresponds qualitatively to an instantaneous current sampled in the middle of the sampling window [17, 19, 31]. The dimensionless peak current depends on the sampling procedure. The relationship between Δi_p and the square root of the frequency depends on the fraction of the pulse at which the current is sampled. This relationship is linear if the relative size of the sampling window is constant. If the absolute size of the sampling window is constant, its relative size increases and the pulse fraction decreases as the frequency is increased. So, the ratio $\Delta i_p/f^{1/2}$ increases with increasing frequency. If the relative size of the sampling window increases from 1% to 7% of the pulse duration, the dimensionless net peak current $\Delta\Phi_p$ increases by 10% [37].

Table II.3.2 Dimensionless peak currents and peak potentials of the forward and the backward components of square-wave voltammograms of fast and reversible redox reaction (II.3.1) ($n\Delta E = 2\,mV$)

nE_{sw}/mV	$\Phi_{p,f}$	$(E_{p,f} - E_{1/2})$/V	$\Phi_{p,b}$	$(E_{p,b} - E_{1/2})$/V
0	0.1201	0.030	–	–
5	0.1590	0.018	–	–
10	0.2011	0.012	–0.0201	−0.026
20	0.2812	0.008	–0.1023	−0.010
30	0.3494	0.006	−0.1815	−0.006
40	0.4035	0.004	−0.2491	−0.004
50	0.4440	0.002	−0.3035	−0.002
60	0.4731	0.002	−0.3456	−0.002
70	0.4933	0.000	−0.3774	0.000
80	0.5069	−0.002	−0.4009	0.002
90	0.5158	−0.004	−0.4182	0.002
100	0.5215	−0.006	−0.4308	0.004

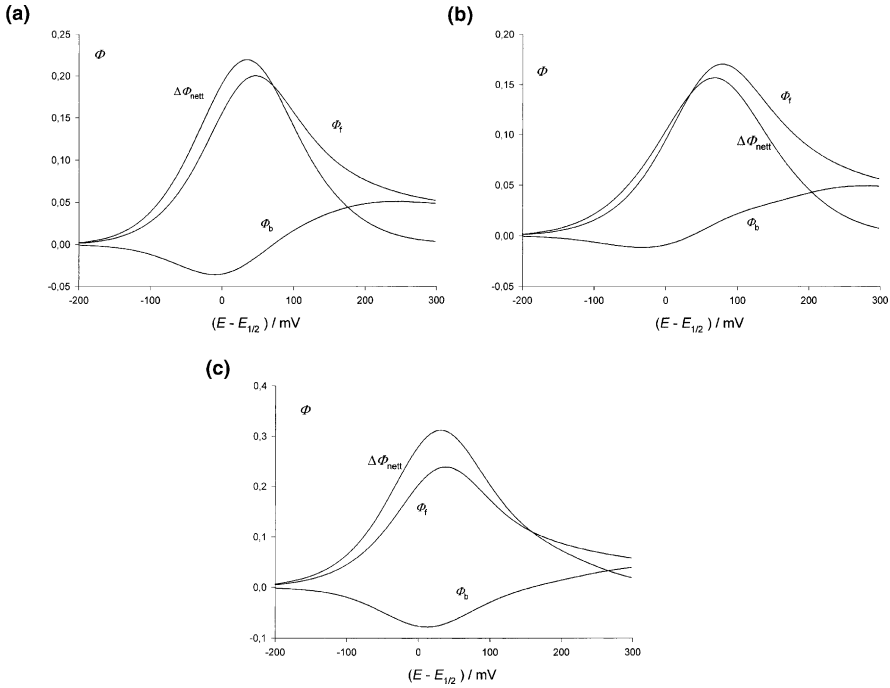

Fig. II.3.3 Square-wave voltammograms of reaction (II.3.1) controlled by electrode kinetics. $n\Delta E = 2$ mV, $nE_{sw} = 50$ mV (**a** and **b**) and 100 *mV* (**c**), $\alpha = 0.5$, $\lambda = 0.1$ (**a**) and 0.05 (**b** and **c**)

If reaction (II.3.1) is controlled by the electrode kinetics (see Chap. I.3), the square-wave response depends on the dimensionless kinetic parameter $\lambda = k_s(D_o f)^{-1/2}(D_o/D_r)^{\alpha/2}$ and the transfer coefficient α [38]. This relationship is shown in the Appendix (see Eqs. II.3.28, II.3.31, II.3.32, and II.3.33). In the quasi-reversible range ($-1.5 < \log\lambda < 0.5$), the dimensionless net peak current $\Delta\Phi_p$ decreases, while both the half-peak width and the net peak potential increase with diminishing λ. These dependencies are not linear, and vary with the transfer coefficient. The real net peak current Δi_p is not a linear function of the square root of frequency [39]. The change in the net response is caused by the transformation of the backward component under the influence of increased frequency. As can be seen in Fig. II.3.3, the minimum gradually disappears as if the amplitude is lessened (compare Figs. II.3.3a, b). The response is very sensitive to a change in the signal parameters, as can be seen by comparing Figs. II.3.3b, c. A complex simulation method based on Eqs. (II.3.31, II.3.32 and II.3.33) was developed and used for the estimation of λ and α parameters of the Zn^{2+}/Zn(Hg) electrode reaction [40–42].

The net current of a totally irreversible electrode reaction (Eq. II.3.1) is smaller than its forward component because the backward component is positive for all potentials (see Fig. II.3.4), regardless of the amplitude [43–45]. The ratio $\Delta i_p/f^{1/2}$ and the half-peak width are both independent of the frequency, but the net

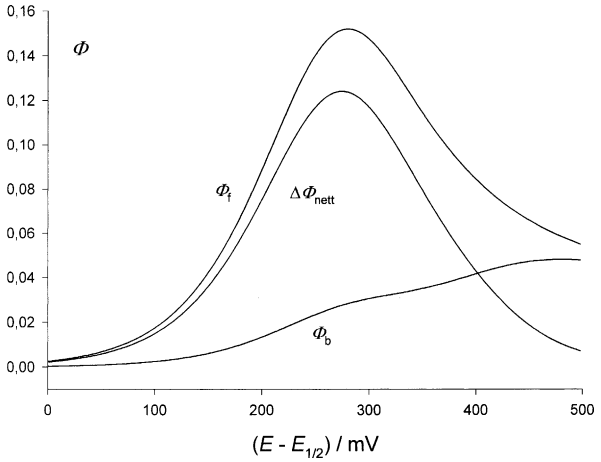

Fig. II.3.4 Square-wave voltammogram of irreversible reaction (II.3.1). $nE_{sw} = 50\,mV$, $n\Delta E = 2\,mV$, $\alpha = 0.5$ and $\lambda = 0.001$

peak potential is a linear function of the logarithm of frequency, with the slope $\partial E_p/\partial \log f = 2.3RT/2\alpha nF$ [6, 38].

II.3.3 Simple Reactions on Stationary Spherical Electrodes and Microelectrodes

The basic theory of SWV at a stationary spherical electrode is explained in the Appendix (see Eqs. II.3.34, II.3.35, II.3.36, II.3.37, II.3.38, II.3.39 and II.3.40). If the electrode reaction (Eq. II.3.1) is fast and reversible, the shape of the SWV response and its peak potential are independent of electrode geometry and size [46–48]. At a spherical electrode the dimensionless net peak current is linearly proportional to the inverse value of the dimensionless electrode radius $y = r^{-1}(D/f)^{1/2}$ [49, 50]. If $n\Delta E = 5\,mV$ and $nE_{sw} = 25\,mV$, the relationship is $\Delta\Phi_p = 0.46 + 0.45y$ [51]. Considering that the surface area of a hemispherical electrode is $S = 2\pi r^2$, the net peak current can be expressed as

$$\Delta i_p = 2.83\,nFc^*D^{1/2}r[1.03rf^{1/2} + D^{1/2}] \qquad \text{(II.3.3)}$$

Theoretically, if an extremely small electrode is used and low frequency is applied, so that $rf^{1/2} \ll D^{1/2}$, a steady-state, frequency-independent peak current should appear: $(\Delta i_p)_{ss} = 2.83\,nFc^*Dr$ [51]. However, even if the electrode radius is as small as 10^{-6} m, the frequency is only 10 Hz, and $D^{1/2}$ is as large as 5×10^{-5} m $s^{-1/2}$, this condition is not fully satisfied. Consequently, SWV measurements at hemispherical microelectrodes are unlikely to be performed under rigorously established steady-state conditions. Moreover, if the frequency is high and a hanging

mercury drop electrode is used, the spherical effect is usually negligible ($y < 10^{-3}$). The relationship between $\Delta\Phi_p$ and $n\Delta E$ and nE_{sw} does not depend on electrode size [48]. The dimensionless net peak current of a reversible reaction (Eq. II.3.1) at an inlaid microdisk electrode is: $\Delta\Phi_p = 0.365 + 0.086\exp(-1.6y) + 0.58y$ (after recalculation to $n\Delta E$ and nE_{sw} as above) [47]. The theoretical steady-state, frequency-independent peak current at this electrode is: $(\Delta i_p)_{ss} = 1.83\,nFDc^*r$, where r is the radius of the disk. At a moderately small inlaid disk electrode, the average dimensionless peak current is: $\Delta\Phi_p = 0.452 + 0.47y$ [47]. Some electroanalytical applications of cylindrical [52, 53] and ring microelectrodes [54] have been described.

The dimensionless peak current of a totally irreversible electrode reaction is a function of the variable y; however, the relationship is not strictly linear. If $\alpha = 0.5$, it can be described with two asymptotes: $\Delta\Phi_p = 0.11 + 0.32y$ (for $y < 0.5$) and $\Delta\Phi_p = 0.15 + 0.24y$ (for $0.5 < y < 10$) . The slopes and intercepts of these straight lines are linear functions of the transfer coefficient α. The responses of quasi-reversible electrode reactions are complex functions of both the electrode radius and the kinetics parameter $\kappa = k_s(Df)^{-1/2}$. Hence, no linear relationship between $\Delta\Phi_p$ and y was found [51].

II.3.4 Reactions of Amalgam-Forming Metals on Thin Mercury Film Electrodes

At a thin mercury film electrode, the dimensionless net peak current $\Delta\Phi_p$ of a reversible redox reaction $M^{n+} + ne^- \rightleftarrows M(Hg)$ depends on the dimensionless film thickness $\Lambda = l(f/D_r)^{1/2}$, where l is the real film thickness [55]. A classical voltammetric experiment was simulated by assuming that no metal atoms are initially present in the film. If $n\Delta E = 10\,\text{mV}$ and $nE_{sw} = 50\,\text{mV}$, $\Delta\Phi_p$ increases from 0.85 (for $\Lambda < 0.1$) to 1.12 (for $\Lambda = 1$) and decreases back to 0.74 for $\Lambda > 5$. The relationship between the real peak current Δi_p and the square root of the frequency is linear only if the parameter Λ remains either smaller than 0.1, or larger than 5 at all frequencies. At moderately thick films these conditions are usually not satisfied [56–58].

At a very thin film ($\Lambda < 0.1$), the real peak current of the reversible reaction (II.3.1) is linearly proportional to the frequency because $\Delta\Phi_p$ linearly depends on the parameter Λ [59, 60]. In reaction (II.3.1), it is assumed that only the species Red is initially present in the solution. This is the condition usually encountered in anodic stripping square-wave voltammetry [Red ≡ M(Hg)]. In the range $0.1 < \Lambda < 5$, $\Delta\Phi_p$ monotonously increases with Λ from 0.03 to 0.74, without a maximum for $\Lambda = 1$. The peak width changes from $99/n$ mV (for $\Lambda < 0.3$) to $124/n$ mV, for $\Lambda > 3$ [60, 61]. Simulations of SWV in the restricted diffusion space were extended to a thin layer cell [62]. The influence of electrode kinetics on direct and anodic stripping SWV on thin mercury film electrodes was analyzed recently [63–65].

SWV can be applied to systems complicated by preceding, subsequent, or catalytic homogeneous chemical reactions [38, 66–69]. Theoretical relationships between the measurable parameters, such as peak shifts, heights and widths, and the appropriate rate constants, were calculated and used for the extraction of kinetic information from the experimental data [66, 67].

II.3.5 Electrode Reactions Complicated by Adsorption of the Reactant and Product

SWV is a very sensitive technique partly because of its ability to discriminate against charging current [70–74]. However, a specific adsorption of reactant may significantly enhance SWV peak currents [75, 76]. Unlike alternating current voltammetry, SWV effectively separates a capacitive current from a so-called pseudocapacitance [77]. This is the basis for an electroanalytical application of SWV in combination with an adsorptive accumulation of analytes [78–81].

A redox reaction of surface-active reactants can be divided in two groups:

$$\mathrm{Ox} \rightleftarrows (\mathrm{Ox})_{\mathrm{ads}} + n\mathrm{e}^- \rightleftarrows (\mathrm{Red})_{\mathrm{ads}} \rightleftarrows \mathrm{Red} \tag{II.3.4}$$

$$\mathrm{Ox} \rightleftarrows (\mathrm{Ox})_{\mathrm{ads}} + n\mathrm{e}^- \rightleftarrows \mathrm{Red} \tag{II.3.5}$$

In the first group the product remains adsorbed on the electrode surface, while in the second group the product is not adsorbed [82]. The reactions of the majority of organic electroactive substances belong to the first group [83]. These are the so-called surface redox reactions. Examples of the second group of reactions are anion-induced adsorption and reduction of amalgam-forming metal ions on mercury electrodes [84–87]. These are mixed redox reactions.

The difference in responses of surface and mixed reactions is most pronounced if the reactions are fast and reversible. The square-wave stripping scan is preceded by a certain accumulation period during which the electrode is charged to the initial potential and the reactant is adsorbed on the electrode surface. The initial potential is rather high, so that only a minute amount of the reactant is reduced. During the stripping process, the equilibrium at the electrode surface is rhythmically disrupted. After each square-wave pulse the redox system tends to reestablish the Nernst equilibrium between Γ_{ox} and Γ_{red} (for the surface reaction), or Γ_{ox} and $c_{\mathrm{red}(x=0)}$ (for the mixed reaction). The current is a measure of the rate of this process (see the Appendix, Eqs. II.3.46 and II.3.47). Besides, the current is caused by the fluxes of dissolved Ox and Red species. If the equilibrium between Γ_{ox} and Γ_{red} is established at the beginning of the pulse, the current sampled at the end of the pulse does not originate from the reduction of initially accumulated reactant, but from the fluxes in the solution. This current is very small because, during the period of adsorptive accumulation, a thick diffusion layer of the reactant has developed and its flux is diminished. Hence, the response is smaller than in direct SWV, without adsorption [88]. In the case of a mixed reaction, the equilibrium between Γ_{ox} and $c_{\mathrm{red}\,(x=0)}$ is

continuously disturbed by the diffusion of Red species from the electrode surface into the solution. For this reason the current sampled at the end of the pulse is proportional to the surface concentration of initially adsorbed reactant [89]. This initial surface concentration is proportional to the bulk concentration of the reactant and the square root of the duration of the accumulation in a solution that is not stirred [78]. The accumulation occurs during the delay time preceding the stripping scan and during the first period of the scan, before the reduction of the reactant:

$$t_{\mathrm{acc}} = t_{\mathrm{delay}} + (E_{\mathrm{p}} - E_{\mathrm{acc}})/f\Delta E \tag{II.3.6}$$

where E_{p} and E_{acc} are the stripping peak potential and the accumulation potential, respectively.

The relationship between the stripping peak current of a fast and reversible mixed reaction and the square-wave frequency is a curve defined by $\Delta i_{\mathrm{p}} = 0$, for $f = 0$, and an asymptote $\Delta i_{\mathrm{p}} = kf + z$ [90]. The intercept z depends on the delay time and apparently vanishes when $t_{\mathrm{delay}} > 30$ s. Consequently, the ratio $\Delta i_{\mathrm{p}}/f$ may not be constant for all frequencies. This effect is caused by the additional adsorption during the first period of the stripping scan. The stripping peak potential of a reversible mixed reaction depends linearly on the logarithm of frequency [89]:

$$\partial E_{\mathrm{p}}/\partial \log f = -2.3RT/2nF \tag{II.3.7}$$

The peak current depends on the square-wave amplitude E_{sw} and the potential increment ΔE in the same way as in the case of the simple reaction (Eq. II.3.1) (see Table II.3.1). The half-peak width also depends on the amplitude and has no diagnostic value. However, the response of the reversible reaction (II.3.5) is narrower than the response of the reversible reaction (Eq. II.3.1). If $nE_{\mathrm{sw}} = 50$ mV and $n\Delta E = 10$ mV, the half-peak widths are 100 mV and 125 mV, respectively [88].

Here it should be mentioned that for the reaction

$$\mathrm{Ox} + n\mathrm{e}^- \rightleftarrows (\mathrm{Red})_{\mathrm{ads}} \rightleftarrows \mathrm{Red} \tag{II.3.8}$$

in which only the reactant Ox is initially present in the solution, but only the product Red is adsorbed, the square-wave peak current depends linearly on the square root of the frequency. The peak potential is a linear function of the logarithm of frequency, with the slope 2.3 $RT/2nF$ [90].

Under the influence of electrode kinetics, the surface reaction (Eq. II.3.4) depends on the dimensionless kinetic parameter $\kappa = k_{\mathrm{s}}/f$ (Eq. II.3.57) and the dimensionless adsorption parameters $a_{\mathrm{ox}} = K_{\mathrm{ox}} f^{1/2} D_{\mathrm{o}}^{-1/2}$ and $a_{\mathrm{red}} = K_{\mathrm{red}} f^{1/2} D_{\mathrm{r}}^{-1/2}$ (Eqs. II.3.58 and II.3.59) [89, 91–93]. Equations (II.3.50) and (II.3.53) are complicated by the diffusion of the redox species Ox and Red and their adsorption equilibria. The kinetic effects can be investigated separately by analyzing a simplified surface reaction (Eq. II.3.64) that is a model of strong and totally irreversible

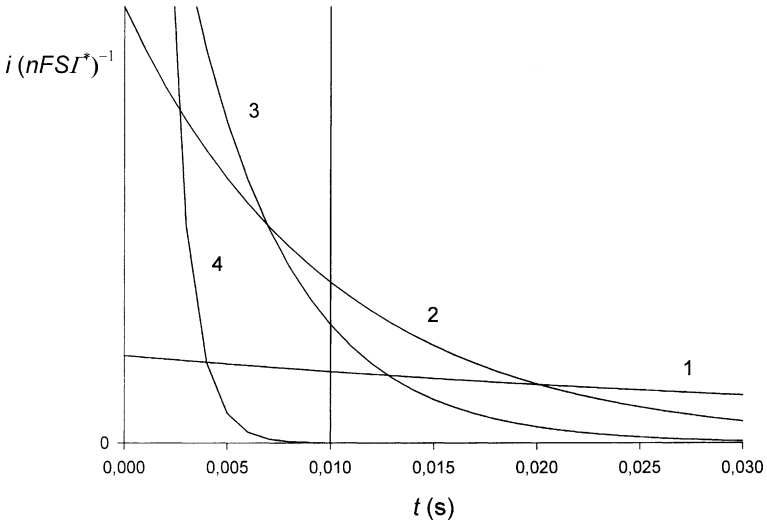

Fig. II.3.5 Chronoamperogram of reaction (II.3.64) (Eq. II.3.74) $E = E^{\ominus}$, $k_s / s^{-1} = 10$ (1), 50 (2), 100 (3) and 500 (4)

adsorption of an electroactive reactant [93, 94]. Under chronoamperometric conditions (for $E = E^{\ominus}$), the current depends exponentially on the product $k_s t$, where t is the time after the application of the potential pulse (see Eq. II.3.74). Figure II.3.5 shows the relationship between the current and the time for different values of the reaction rate constant. The vertical bar denotes the pulse duration $t_p = 10$ ms. If the k_s value is very large (curve 4, $k_s = 500\ s^{-1}$), the current quickly decreases and virtually vanishes before the end of the pulse. This is the response of a fast and reversible surface reaction as discussed above. The current caused by a slower reaction declines less rapidly. After 10 ms, the highest current corresponds to $k_s = 50\ s^{-1}$, while both faster ($k_s = 100\ s^{-1}$) and slower ($k_s = 10\ s^{-1}$) charge transfers cause lower currents. The first derivative of Eq. (II.3.74) shows that $k_{s,max} = (2t_p)^{-1}$. This is the rate constant of a kinetically controlled electrode reaction that gives a maximum response at the end of the pulse. Equations (II.3.75), (II.3.76), (II.3.77), (II.3.78), (II.3.79) and (II.3.80) show the general relationship between the dimensionless chronoamperometric response (Eq. II.3.71) and the dimensionless kinetic parameter $\lambda = k_s t$. At any electrode potential there is a certain λ_{max} giving the maximum response. The numerical analysis (Eq. II.3.69) of a SWV of a surface reaction (Eq. II.3.64) is shown in Fig. II.3.6. The dimensionless peak current $\Delta\Phi_p = \Delta i_p (nFS\Gamma^*_{ox} f)^{-1}$ is plotted as a function of the logarithm of the dimensionless kinetic parameter $\kappa = k_s / f$. The peak currents of quasi-reversible surface redox reactions are much higher than the peak currents of both reversible and totally irreversible surface reactions. The same relationship was found in SWV of the surface reaction (Eq. II.3.4) if $0.1 < a_{ox}/a_{red} \leq 10$ (see Eqs. II.3.50 and II.3.53). This is

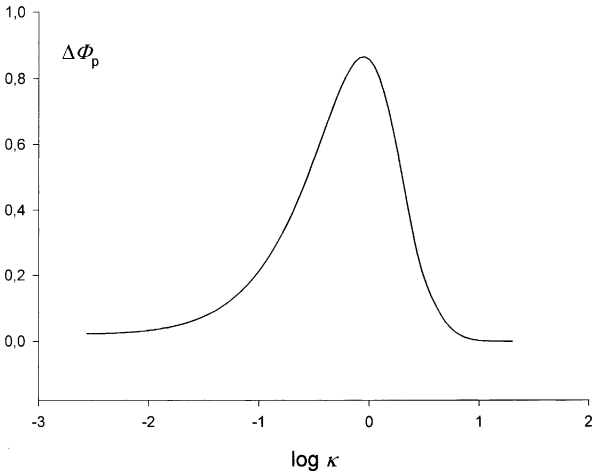

Fig. II.3.6 Theoretical quasi-reversible maximum in SWV. A dependence of the dimensionless net peak current $\Delta\Phi_p = \Delta i_p(nFS\Gamma^*_{ox}f)^{-1}$ on the logarithm of dimensionless kinetic parameter $\kappa = k_s/f$ (*Eq.* II.3.69). $n\Delta E = 2$ mV, $nE_{sw} = 50$ mV, $\alpha = 0.5$, and M = 50

called the quasi-reversible maximum in SWV [93, 95]. The critical dimensionless rate constant κ_{max} depends on the transfer coefficient α and the product nE_{sw}, but does not depend on the surface concentration of the adsorbed reactant if there are no interactions between the molecules of the deposit. Values of κ_{max} are listed in Table II.3.3 [96].

A variation in frequency changes the apparent reversibility of the surface reaction (Eq. II.3.4) [91, 92]. The reaction appears reversible if $k_s/f > 5$, and totally irreversible if $k_s/f < 10^{-2}$. The ratio of the real peak current and the corresponding frequency ($\Delta i_p/f$) increases with increasing frequency if $1 < \kappa < 5$, but it decreases if $10^{-2} < \kappa < 1$. Hence, the ratio $\Delta i_p/f$ may depend parabolically on the logarithm

Table II.3.3 Dependence of the critical kinetic parameter κ_{max} on the normalized square-wave amplitude nE_{sw} and the transfer coefficient α

κ_{max}					
α	nE_{sw}/mV				
	15	25	30	40	50
0.1	1.43	1.35	1.38	1.33	1.26
0.2	1.32	1.30	1.25	1.17	1.08
0.3	1.31	1.26	1.20	1.10	0.97
0.4	1.29	1.20	1.16	1.04	0.90
0.5	1.28	1.19	1.13	1.01	0.88
0.6	1.27	1.18	1.13	1.02	0.89
0.7	1.26	1.22	1.17	1.04	0.94
0.8	1.25	1.24	1.19	1.12	1.04
0.9	1.25	1.27	1.30	1.26	1.19

of frequency. The characteristic frequency f_{max} of the maximum ratio $(\Delta i_p/f)_{max}$ is related to the standard reaction rate constant by the equation: $k_s = \kappa_{max} f_{max}$, where κ_{max} depends on the experimental conditions (see Table II.3.3). If the transfer coefficient α is not known, an average value of κ_{max} can be used [96]. The kinetic parameters of electrode reactions of adsorbed alizarin red S [97], europium(III)–salicylate complex [98], probucole [99], azobenzene [96], 6-propyl-2-thiouracil [100], and indigo [101] were determined by this method.

The response of the fast and reversible surface reaction (Eq. II.3.4) splits into two peaks if $nE_{sw} > 40$ mV [89, 91, 92, 102]. The splitting is shown in Fig. II.3.7 a for the reaction: $(Red)_{ads} \rightleftarrows (Ox)_{ads} + ne^-$. It was observed in SWV of adsorbed methylene blue [89], cytochrome *c* [92], azobenzene [91], and alizarin red S [102]. The separation between the anodic and cathodic components of the response is a consequence of the current sampling procedure. The ratio between the cathodic and anodic peak currents of the net response depends on the transfer coefficient [102]:

$$\Delta\Phi_{p,c}/\Delta\Phi_{p,a} = 5.64 \exp(-3.46\,\alpha) \tag{II.3.9}$$

If $\alpha = 0.5$ these two peaks are equal. The peak potentials of the net response are independent of the frequency, regardless of the amplitude, if $\kappa > 5$.

Figure II.3.7b–d shows the changes in the cathodic and anodic components of the net response in the range of the quasi-reversible maximum. These currents are very sensitive to a change in frequency and allowed the evaluation of kinetic parameters of azobenzene [91], cytochrome *c* [92], and Cu(II)-oxine complexes [103] by fitting experimental data with theoretical curves. In addition, a theory of a two-step surface reaction was developed and applied to the kinetics of the reduction of adsorbed 4-(dimethylamino)azobenzene [104].

The SWV response of the mixed reaction (Eq. II.3.5) influenced by the electrode kinetics depends on the complex dimensionless parameter $K_{kin} = k_s K_{ox} r_s^{-1/2} D^{-1/4} f^{-3/4}$, where k_s and r_s are defined by the equation:

$$i/nFS = k_s \exp(-\alpha\varphi)[\Gamma_{ox} - r_s(c_{red})_{x=0} \exp\varphi] \tag{II.3.10}$$

and K_{ox} is the adsorption constant (Eq. II.3.43). The dimensionless peak current $\Delta\Phi_p = \Delta i_p (nFSK_{ox} c^*_{ox} f)^{-1}$ is independent of the kinetic parameter if either log $K_{kin} > 1.5$ (reversible reactions) or log $K_{kin} < -1.5$ (totally irreversible reactions). In the range $-1.5 <$ log $K_{kin} < 1.5$, the quasi-reversible maximum appears [105–107]. The critical kinetic parameter, $K_{kin,max}$, depends on the product nE_{sw} and the transfer coefficient α [107]. It can be used for an estimation of rate constants of mixed reactions [98].

A special case of mixed reactions is an accumulation of insoluble mercuric and mercurous salts on the mercury electrode surface and their stripping off by SWV:

$$HgL(s) \rightleftarrows Hg(l) + L^{2-}(aq) + 2e^- \tag{II.3.11}$$

$$Hg_2X_2(s) \rightleftarrows 2Hg(l) + 2X^- + 2e^- \tag{II.3.12}$$

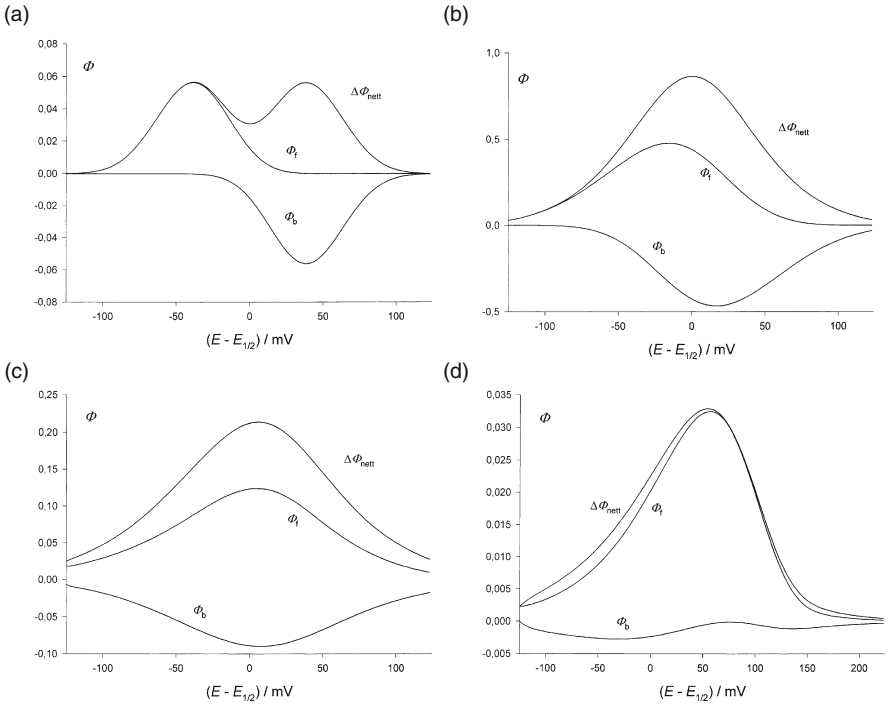

Fig. II.3.7 Theoretical square-wave voltammograms of a kinetically controlled reaction (Eq. II.3.64). $n\Delta E = 2$ mV, $nE_{sw} = 50$ mV, $\alpha = 0.5$ and $\kappa = 5$ (**a**), 0.9 (**b**), 0.1 (**c**) and 0.01 (**d**)

The quasi-reversible maxima in SWV of first-order [106, 107] and second-order [108] mixed reactions were analyzed. If the ligand L^{2-} in Eq. (II.3.11) remains adsorbed on the electrode surface, the mixed reaction turns into a surface reaction and the response changes accordingly [100].

SWV responses of totally irreversible surface and mixed reactions are identical [78, 89, 109, 110]. The real peak current is linearly proportional to the frequency, while the peak potential depends linearly on the logarithm of frequency, with the slope:

$$\partial E_p/\partial \log f = -2.3RT/\alpha nF \qquad \text{(II.3.13)}$$

The half-peak width is independent of the amplitude if $nE_{sw} > 20$ mV [109]:

$$\Delta E_{p/2} = (63.5 \pm 0.5)/\alpha n \,\text{mV} \qquad \text{(II.3.14)}$$

II.3.6 Applications of Square-Wave Voltammetry

SWV has been applied in numerous electrochemical and electroanalytical measurements [2, 4, 6, 7]. Apart from the investigation of charge transfer kinetics of dissolved zinc ions [40, 42] and adsorbed organic species mentioned above [91, 92, 96–101, 103, 110], the mechanisms of redox reactions of titanium(III), iron(II) [66] and adsorbed metal complexes [77, 84–87] were analyzed. Electroanalytical application of SWV can be divided into direct and stripping measurements. Analytes measured directly, without accumulation, were Bi(III), Cu(II), Pb(II), Tl(I), In(III), Cd(II), Zn(II), Fe(III/II)oxalate [18], Ni(II) [36], tert-butyl hydroperoxide and *N*-acetylpenicillamine thionitrite [44]. The stripping measurements were based either on the accumulation of amalgams [18, 111, 112] and metal deposits on solid electrodes [52, 113], or on the adsorptive accumulation of organic substances [114] and metal complexes [115]. Anodic stripping SWV was applied to thin mercury film covered macro electrodes [116] and micro electrodes [52, 117]. Some examples of stripping SWV with adsorptive accumulation include the analyses of cimetidine [78], nicotinamide adenine dinucleotide [79, 80], berberine [81, 109], azobenzene [83], sulfide [106], and cysteine [108]. Other examples can be found in Table II.3.4.

Finally, SWV was used for the detection of heavy metals in thin-layer chromatography [118] and various organic substances in high-performance liquid chromatography [119].

Table II.3.4 Some elements and compounds measured by square-wave voltammetry

Reactant	Footnote	Reactant	Footnote
Bismuth	F1	Captopril	F28
Cadmium	F2	Cocaine	F29
Chromium	F3	Cytochrome	F30
Copper	F4	Daminozide	F31
Europium	F5	Dimethoate	F32
Germanium	F6	Dopamine	F33
Gold	F7	Famotidine	F34
Indium	F8	Fluorouracil	F35
Iodine	F9	Folic acid	F36
Lead	F10	Hemoglobin	F37
Manganese	F11	Hydroxypyrene	F38
Mercury	F12	Melatonin	F39
Molybdenum	F13	Mifepristone	F40
Nickel	F14	Molinate	F41
Ruthenium	F15	Nitrophenol	F42
Selenium	F16	Nitroprusside	F43
Thallium	F17	Orthochlorophenol	F44
Uranium	F18	Quinoxaline	F45
Zinc	F19	Serotonin	F46
Adenosine	F20	Sulfadimetoxol	F47
Ametryne	F21	Sulfaquinoxaline	F48

Table II.3.4 (continued)

Reactant	Footnote	Reactant	Footnote
Amisulpride	F22	Sunset yellow	F49
Azidothymidine	F23	Tetramethrin	F50
Azithromycin	F24	Toxogonin	F51
Benzaldehyde	F25	Uric acid	F52
Benzoylecgonine	F26	Venlafaxine	F53
Caffeine	F27	Warfarin	F54

(F1) Komorsky-Lovrić Š (1988) Anal Chim Acta 204: 161 (F2) Yantasee W, Lin Y, Fryxell GE, Busche BJ (2004) Anal Chim Acta 502: 207 (F3) Boussemart M, van den Berg CMG, Ghaddaf M (1992) Anal Chim Acta 262: 103 (F4) Hardcastle JL, Compton RG (2002) Electroanalysis 14: 753 (F5) Zelić M (2003) Croat Chem Acta 76: 241 (F6) Sohn SC, Park YJ, Joe KS (1997) J Korean Chem Soc 41: 590 (F7) Riley JP, Wallace GG (1991) Electroanalysis 3: 191 (F8) Zelić M, Mlakar M, Branica M (1994) Anal Chim Acta 289: 299 (F9) Wong GTF, Zhang LS (1992) Talanta 39: 355 (F10) Richter EM, Pedrotti JJ, Angnes L (2003) Electroanalysis 15: 1871 (F11) Komorsky-Lovrić Š (1998) Croat Chem Acta 71: 263 (F12) Walcarius A, Devoy J, Bessiere J (2000) J Solid State Electrochem 4: 330 (F13) Quentel F, Mirčeski V (2004) Electroanalysis 16: 1690 (F14) Morfobos M, Economou A, Voulgaropoulos A (2004) Anal Chim Acta 519: 57 (F15) Prakash R, Tyagi B, Ramachandraiah G (1997) Indian J Chem A 36: 201 (F16) Tan SH, Kounaves SP (1998) Electroanalysis 10: 364 (F17) Zen J-M, Wu J-W (1997) Electroanalysis 9: 302 (F18) Mlakar M (1993) Anal Chim Acta 276: 367 (F19) Demetriades D, Economou A, Voulgaropoulos A (2004) Anal Chim Acta 519: 167 (F20) Flores JR, Alvarez JMF (1992) Electroanalysis 4: 347 (F21) Cabral MF, de Souza D, Alves CR, Machado SAS (2003) Eclet Quim 28: 41 (F22) Özkan SA, Uslu B, Sentürk Z (2004) Electroanalysis 16: 231 (F23) Vacek J, Andrysik Z, Trnkova L, Kizek R (2004) Electroanalysis 16: 224 (F24) Farghaly OAE-M, Mohamed NAL (2004) Talanta 62: 531 (F25) Saska M, Sturrock PE (1983) Anal Chim Acta 155: 243 (F26) Komorsky-Lovrić Š, Gagić S, Penovski R (1999) Anal Chim Acta 389: 219 (F27) Zen J-M, Ting Y-S (1998) Analyst 123: 1145 (F28) Parham H, Zargar B (2005) Talanta 65: 776 (F29) Pavlova V, Mirčeski V, Komorsky-Lovrić Š, Petrovska-Jovanović S, Mitrevski B (2004) Anal Chim Acta 512: 49 (F30) Bianco P, Lattuca C (1997) Anal Chim Acta 353: 53 (F31) Ianniello RM (1987) Anal Chim Acta 193: 81 (F32) Hernandez P, Ballesteros Y, Galan F, Hernandez L (1994) Electroanalysis 6: 51 (F33) Zen J-M, Chen I-L (1997) Electroanalysis 9: 537 (F34) Mirčeski V, Jordanoski B, Komorsky-Lovrić Š (1998) Portugaliae Electrochim Acta 16: 43 (F35) Mirčeski V, Gulaboski R, Jordanoski B, Komorsky-Lovrić Š (2000) J Electroanal Chem 490: 37 (F36) Cakir S, Atayman I, Cakir O (1997) Mikrochim Acta 126: 237 (F37) Liu H, Hu N (2003) Anal Chim Acta 481: 91 (F38) Castro AA, Wagener ALR, Farias PAM, Bastos MB (2004) Anal Chim Acta 521: 201 (F39) Beltagi AM, Khashaba PY, Ghoneim MM (2003) Electroanalysis 15: 1121 (F40) Rodriguez J, Berzas JJ, Castaneda G, Rodriguez N (2004) Electroanalysis 16: 661 (F41) Oliveira Brett AM, Garrido EM, Lima JLFC, Delerue-Matos C (1997) Portugaliae Electrochim Acta 15: 315 (F42) Pedrosa VA, Codognoto L, Avaca LA (2003) J Braz Chem Soc 14: 530 (F43) Carapuca HM, Simao JEJ, Fogg AG (1998) J Electroanal Chem 455: 93 (F44) Manisankar P, Prabu HG (1995) Electroanalysis 7: 594 (F45) Barros AA, Rodrigues JA, Almeida PJ, Rodrigues PG, Fogg AG (1999) Anal Chim Acta 385: 315 (F46) Zen J-M, Chen I-L, Shih Y (1998) Anal Chim Acta 369: 103 (F47) Berzas JJ, Rodrigues J, Lemus JM, Castaneda G (1997) Electroanalysis 9: 474 (F48) Berzas JJ, Rodriguez J, Lemus JM, Castaneda G (1993) Anal Chim Acta 273: 369 (F49) Berzas Nevado JJ, Rodrigues Flores J, Villasenor Llerena MJ (1997) Talanta 44: 467 (F50) Hernandez P, Galan-Estella F, Hernandez L (1992) Electroanalysis 4: 45 (F51) Komorsky-Lovrić Š (1990) J Electroanal Chem 289: 161 (F52) Zen J-M, Chen P-J (1997) Anal Chem 69: 5087 (F53) Lima JLFC, Loo DV, Delerue-Matos C, Roque Da Silva AS (1999) Farmaco 54: 145 (F54) Ghoneim MM, Tawfik A (2004) Anal Chim Acta 511: 63

Appendix

(A) For a stationary planar diffusion model of a simple redox reaction (Eq. II.3.1) the following differential equations and boundary conditions can be formulated:

$$\frac{\partial c_{\mathrm{red}}}{\partial t} = D_{\mathrm{r}} \frac{\partial^2 c_{\mathrm{red}}}{\partial x^2} \tag{II.3.15}$$

$$\frac{\partial c_{\mathrm{ox}}}{\partial t} = D_{\mathrm{o}} \frac{\partial^2 c_{\mathrm{ox}}}{\partial x^2} \tag{II.3.16}$$

$$t = 0, x \geq 0\text{: } c_{\mathrm{red}} = c^*, c_{\mathrm{ox}} = 0 \tag{II.3.17}$$

$$t > 0, x \to \infty, c_{\mathrm{red}} \to c^*, c_{\mathrm{ox}} \to 0 \tag{II.3.18}$$

$$x = 0\text{: } D_{\mathrm{r}} \left(\frac{\partial c_{\mathrm{red}}}{\partial x} \right)_{x=0} = \frac{i}{nFS} \tag{II.3.19}$$

$$D_{\mathrm{o}} \left(\frac{\partial c_{\mathrm{ox}}}{\partial x} \right)_{x=0} = -\frac{i}{nFS} \tag{II.3.20}$$

If reaction (II.3.1) is fast and reversible, the Nernst equation has to be satisfied:

$$(c_{\mathrm{ox}})_{x=0} = (c_{\mathrm{red}})_{x=0} \exp(\varphi) \tag{II.3.21}$$

$$\varphi = \frac{nF}{RT}(E - E^{\ominus}) \tag{II.3.22}$$

If reaction (II.3.1) is kinetically controlled, the Butler-Volmer equation applies:

$$\frac{i}{nFS} = -k_{\mathrm{s}} \exp(-\alpha\varphi)[(c_{\mathrm{ox}})_{x=0} - (c_{\mathrm{red}})_{x=0} \exp(\varphi)] \tag{II.3.23}$$

where c_{red} and c_{ox} are the concentrations of the reduced and oxidized species, respectively. D_{r} and D_{o} are the corresponding diffusion coefficients, k_{s} is the standard rate constant, α is the transfer coefficient, $E^{\ominus}$ is the standard potential, x is the distance from the electrode surface, t is the time variable, and the other symbols are explained below Eq. (II.3.1) above.

The solution of Eqs. (II.3.15), (II.3.16), (II.3.17), (II.3.18), (II.3.19), (II.3.20), (II.3.21) and (II.3.22) is an integral equation [120]:

$$\int_0^t \Phi^*[\pi(t-\tau)]^{-1/2} \mathrm{d}\tau = \exp(\varphi^*)[1 + \exp(\varphi^*)]^{-1} \tag{II.3.24}$$

where

$$\Phi^* = i[nFSc^* D_r^{1/2}]^{-1} \tag{II.3.25}$$

$$\varphi^* = nF(E - E_{1/2})/RT \tag{II.3.26}$$

$$E_{1/2} = E^{\ominus} + RT[\ln(D_r/D_o)]/2nF \tag{II.3.27}$$

The solution for the kinetically controlled reaction is [120]:

$$\Phi^* = -\lambda^* \exp\left(-\alpha\varphi^*\right)\left[1 + \exp\left(\varphi^*\right)\right] \int_0^t \Phi^* [\pi\,(t-\tau)]^{-1/2}\,\mathrm{d}\tau + \lambda^* \exp\left[(1-\alpha)\,\varphi^*\right] \tag{II.3.28}$$

The convolution integrals in Eqs. (II.3.24) and (II.3.28) can be solved by the method of numerical integration proposed by Nicholson and Olmstead [38, 121]:

$$\int_0^t \Phi^* [\pi\,(t-\tau)]^{-1/2}\mathrm{d}\tau = 2\,(d/\pi)^{1/2} \sum_{j=1}^{m} \Phi_j^* S_{m-j+1} \tag{II.3.29}$$

where d is the time increment, $t = md$, Φ_j^* is the average value of the function Φ^* within the j^{th} time increment, $S_k = k^{1/2} - (k-1)^{1/2}$ and $S_1 = 1$. Each square-wave half-period is divided into 25 time increments: $d = (50\,f)^{-1}$. By this method, Eq. (II.3.24) is transformed into the system of recursive formulae:

$$\Phi_m = 5\,(\pi/2)^{1/2} \exp\left(\varphi_m^*\right)\left[1 + \exp\left(\varphi_m^*\right)\right]^{-1} - \sum_{j=1}^{m-1} \Phi_j S_{m-j+1} \tag{II.3.30}$$

where $\Phi = i[nFSc^*(D_r f)^{1/2}]^{-1}, \varphi_m^* = nF(E_m - E_{1/2})/RT, m = 1,2,3,\ldots \mathrm{M}$ and $\mathrm{M} = 50\,(E_{\text{fin}} - E_{\text{st}})/\Delta E$. The potential E_m changes from $E_{\text{stair}} = E_{\text{st}}$ to $E_{\text{stair}} = E_{\text{fin}}$ according to Fig. II.3.1. The recursive formulae for the kinetically controlled reaction are [38, 40, 41, 44]:

$$\Phi_m = Z_1 - Z_2 \sum_{j=1}^{m-1} \Phi_j S_{m-j+1} \tag{II.3.31}$$

$$Z_1 = \frac{\lambda \exp\left[(1-\alpha)\varphi_m^*\right]}{1 + \frac{\lambda\sqrt{2}}{5\sqrt{\pi}}\left[\exp\left(-\alpha\varphi_m^*\right) + \exp\left((1-\alpha)\varphi_m^*\right)\right]} \tag{II.3.32}$$

$$Z_2 = \frac{\frac{\lambda\sqrt{2}}{5\sqrt{\pi}}\left[\exp\left(-\alpha\varphi_m^*\right) + \exp\left((1-\alpha)\varphi_m^*\right)\right]}{1 + \frac{\lambda\sqrt{2}}{5\sqrt{\pi}}\left[\exp\left(-\alpha\varphi_m^*\right) + \exp\left((1-\alpha)\varphi_m^*\right)\right]} \tag{II.3.33}$$

where

$$\lambda = \frac{k_s}{\sqrt{D_o f}} \left(\frac{D_o}{D_r}\right)^{\frac{\alpha}{2}}$$

is a dimensionless kinetic parameter.

(B) On a stationary spherical electrode, a simple redox reaction

$$\mathrm{Ox} + n\mathrm{e}^- \leftrightarrows \mathrm{Red} \tag{II.3.34}$$

can be mathematically represented by the well-known integral equation [120]:

$$\Phi = \frac{k_s}{(Df)^{1/2}} \exp(-\alpha\varphi)[1 - f^{1/2}(1 + \exp(\varphi))I^o] \tag{II.3.35}$$

$$\Phi = i(nFSc^*_{ox})^{-1}(Df)^{-1/2} \tag{II.3.36}$$

$$I^o = \int_0^t \Phi[\pi(t-u)]^{-1/2}\mathrm{d}u - \frac{D^{1/2}}{r}\int_0^t \Phi \exp[D(t-u)r^{-2}]\mathrm{erfc}[D^{1/2}r^{-1}(t-u)^{1/2}]\mathrm{d}u \tag{II.3.37}$$

where r is the radius of the spherical electrode and c^*_{ox} is the bulk concentration of the oxidized species. The meanings of all other symbols are as above. It is assumed that both the reactant and product are soluble, that only the oxidized species is initially present in the solution, and that the diffusion coefficients of the reactant and product are equal. For numerical integration, Eq. (II.3.35) can be transformed into a system of recursive formulae [51]:

$$\Phi_m = \frac{-\frac{D^{1/2}}{rf^{1/2}} - (1 + \exp(\varphi_m)) \sum_{i=1}^{m-1} \Phi_i S_{m-i+1}}{\frac{D}{k_s r}\exp(\alpha\varphi_m) + S_1\,(1 + \exp(\varphi_m))} \tag{II.3.38}$$

$$S_1 = 1 - \exp(Df^{-1}r^{-2}N^{-1})\mathrm{erfc}(D^{1/2}f^{-1/2}r^{-1}N^{-1/2}) \tag{II.3.39}$$

$$\begin{aligned} S_k = {} & \exp\left[Df^{-1}r^{-2}N^{-1}\,(k-1)\right]\mathrm{erfc}\left[D^{1/2}f^{-1/2}r^{-1}N^{-1/2}\,(k-1)^{1/2}\right] \\ & - \exp\left(Df^{-1}r^{-2}N^{-1}k\right)\mathrm{erfc}\left(D^{1/2}f^{-1/2}r^{-1}N^{-1/2}k^{1/2}\right) \end{aligned} \tag{II.3.40}$$

where N is the number of time increments in each square-wave period. The ratio $k_s\,r/D$ is the dimensionless standard charge transfer rate constant of reaction (II.3.34) and the ratio $rf^{1/2}/D^{1/2}$ is the dimensionless electrode radius.

(C) A surface redox reaction (II.3.4) on a stationary planar electrode is represented by the system of differential equations (II.3.15) and (II.3.16), with the following initial and boundary conditions [89]:

$$t = 0, x \geq 0 : c_{\mathrm{ox}} = c_{\mathrm{ox}}^{*}, c_{\mathrm{red}} = 0,\ \Gamma_{\mathrm{ox}} = \Gamma_{\mathrm{red}} = 0 \tag{II.3.41}$$

$$t > 0 : x \to \infty : c_{\mathrm{ox}} \to c_{\mathrm{ox}}^{*},\ c_{\mathrm{red}} \to 0 \tag{II.3.42}$$

$$x = 0 : K_{\mathrm{ox}}(c_{\mathrm{ox}})_{x=0} = \Gamma_{\mathrm{ox}} \tag{II.3.43}$$

$$K_{\mathrm{red}}(c_{\mathrm{red}})_{x=0} = \Gamma_{\mathrm{red}} \tag{II.3.44}$$

$$i/nFS = k_{\mathrm{s}} \exp(-\alpha\varphi)[\Gamma_{\mathrm{ox}} - \exp(\varphi)\Gamma_{\mathrm{red}}] \tag{II.3.45}$$

$$D_{\mathrm{o}}(\partial c_{\mathrm{ox}}/\partial x)_{x=0} = d\Gamma_{\mathrm{ox}}/dt + i/nFS \tag{II.3.46}$$

$$D_{\mathrm{r}}(\partial c_{\mathrm{red}}/\partial x)_{x=0} = d\Gamma_{\mathrm{red}}/dt - i/nFS \tag{II.3.47}$$

$$\varphi = nF(E - E^{\ominus}_{\Gamma_{\mathrm{ox}}/\Gamma_{\mathrm{red}}})/RT \tag{II.3.48}$$

$$E^{\ominus}_{\Gamma_{\mathrm{ox}}/\Gamma_{\mathrm{red}}} = E^{\ominus} + (RT/nF)\ln(K_{\mathrm{red}}/K_{\mathrm{ox}}) \tag{II.3.49}$$

where Γ_{ox} and Γ_{red} are the surface concentrations of the oxidized and reduced species, respectively, and K_{ox} and K_{red} are the constants of linear adsorption isotherms. The solution of Eqs. (II.3.15) and (II.3.16) is an integral equation:

$$\begin{aligned} &i/nFS = k_{\mathrm{s}} \exp(-\alpha\varphi) \\ &\left\{K_{\mathrm{ox}} c_{\mathrm{ox}}^{*}\left[1 - \exp\left(D_{\mathrm{o}} t K_{\mathrm{ox}}^{-2}\right)\mathrm{erfc}\left(D_{\mathrm{o}}^{1/2} t^{1/2} K_{\mathrm{ox}}^{-1}\right)\right] - I_{\mathrm{ox}} - I_{\mathrm{red}} \exp(\varphi)\right\} \end{aligned} \tag{II.3.50}$$

$$I_{\mathrm{ox}} = \int_0^t (i/nFS) \exp\left[D_{\mathrm{o}}(t-\tau) K_{\mathrm{ox}}^{-2}\right]\mathrm{erfc}\left[D_{\mathrm{o}}^{1/2}(t-\tau)^{1/2} K_{\mathrm{ox}}^{-1}\right] \mathrm{d}\tau \tag{II.3.51}$$

$$I_{\mathrm{red}} = \int_0^t (i/nFS) \exp\left[D_{\mathrm{r}}(t-\tau) K_{\mathrm{red}}^{-2}\right]\mathrm{erfc}\left[D_{\mathrm{r}}^{1/2}(t-\tau)^{1/2} K_{\mathrm{red}}^{-1}\right] \mathrm{d}\tau \tag{II.3.52}$$

For numerical integration, Eqs. (II.3.50), (II.3.51) and (II.3.52) are transformed into a system of recursive formulae [93]:

$$\Phi_{\mathrm{m}} = \frac{\kappa \exp(-\alpha\varphi_m)\left[1 - \exp\left(a_{\mathrm{ox}}^{-2} m N^{-1}\right)\mathrm{erfc}\left(a_{\mathrm{ox}}^{-1} m^{1/2} N^{-1/2}\right) - SS_1 + SS_2\right]}{1 + \kappa \exp(-\alpha\varphi_m)\left[2(N\pi)^{-1/2}(a_{\mathrm{ox}} + a_{\mathrm{red}} \exp(\varphi_m)) - a_{\mathrm{ox}}^{2} M_1 - a_{\mathrm{red}}^{2} \exp(\varphi_m) P_1\right]} \tag{II.3.53}$$

$$SS_1 = 2(N\pi)^{-1/2}\left[a_{\mathrm{ox}} + a_{\mathrm{red}} \exp(\varphi_m)\right] \sum_{j=1}^{m-1} \Phi_j S_{m-j+1} \tag{II.3.54}$$

$$SS_2 = \sum_{j=1}^{m-1} \Phi_j \left[a_{\mathrm{ox}}^2 M_{m-j+1} + a_{\mathrm{red}}^2 \exp(\varphi_m) P_{m-j+1} \right] \tag{II.3.55}$$

$$\Phi = i \left(nFSK_{\mathrm{ox}} c_{\mathrm{ox}}^* f \right)^{-1} \tag{II.3.56}$$

$$\kappa = k_{\mathrm{s}}/f \tag{II.3.57}$$

$$a_{\mathrm{ox}} = K_{\mathrm{ox}} f^{1/2} D_{\mathrm{o}}^{-1/2} \tag{II.3.58}$$

$$a_{\mathrm{red}} = K_{\mathrm{red}} f^{1/2} D_{\mathrm{r}}^{-1/2} \tag{II.3.59}$$

$$d = N^{-1} f^{-1} \tag{II.3.60}$$

$$S_k = k^{1/2} - (k-1)^{1/2} \tag{II.3.61}$$

$$M_1 = 1 - \exp\left(a_{\mathrm{ox}}^{-2} N^{-1} \right) \operatorname{erfc}\left(a_{\mathrm{ox}}^{-1} N^{-1/2} \right)$$

$$\begin{aligned} M_k = {} & \exp\left[a_{\mathrm{ox}}^{-2} (k-1) N^{-1} \right] \operatorname{erfc}\left[a_{\mathrm{ox}}^{-1} (k-1)^{1/2} N^{-1/2} \right] \\ & - \exp\left[a_{\mathrm{ox}}^{-2} k N^{-1} \right] \operatorname{erfc}\left[a_{\mathrm{ox}}^{-1} k^{1/2} N^{-1/2} \right] \end{aligned} \tag{II.3.62}$$

$$P_1 = 1 - \exp\left(a_{\mathrm{red}}^{-2} N^{-1} \right) \operatorname{erfc}\left(a_{\mathrm{red}}^{-1} N^{-1/2} \right)$$

$$\begin{aligned} P_k = {} & \exp\left[a_{\mathrm{red}}^{-2} (k-1) N^{-1} \right] \operatorname{erfc}\left[a_{\mathrm{red}}^{-1} (k-1)^{1/2} N^{-1/2} \right] \\ & - \exp\left[a_{\mathrm{red}}^{-2} k N^{-1} \right] \operatorname{erfc}\left[a_{\mathrm{red}}^{-1} k^{1/2} N^{-1/2} \right] \end{aligned} \tag{II.3.63}$$

(D) In a simplified approach to the surface redox reaction, the transport of Ox and Red in the solution is neglected. This assumption corresponds to a totally irreversible adsorption of both redox species [94]:

$$(\mathrm{Ox})_{\mathrm{ads}} + n\mathrm{e}^- \rightleftarrows (\mathrm{Red})_{\mathrm{ads}} \tag{II.3.64}$$

The current is determined by Eq. (II.3.45), with the initial and boundary conditions:

$$t = 0, \Gamma_{\mathrm{ox}} = \Gamma_{\mathrm{ox}}^*, \Gamma_{\mathrm{red}} = 0 \tag{II.3.65}$$

$$t > 0 : \Gamma_{\mathrm{ox}} + \Gamma_{\mathrm{red}} = \Gamma_{\mathrm{ox}}^* \tag{II.3.66}$$

$$\mathrm{d}\Gamma_{\mathrm{ox}}/\mathrm{d}t = -i/nFS \tag{II.3.67}$$

$$\mathrm{d}\Gamma_{\mathrm{red}}/\mathrm{d}t = i/nFS \tag{II.3.68}$$

The solution of Eq. (II.3.45) is a system of recursive formulae:

$$\phi_{\mathrm{m}} = \frac{\kappa \exp(-\alpha\varphi_m)\left[1 - N^{-1}(1+\exp(\varphi_m))\sum_{j=1}^{m-1}\Phi_j\right]}{1+\kappa\exp(-\alpha\varphi_m)N^{-1}(1+\exp(\varphi_m))} \tag{II.3.69}$$

$$\Phi = \frac{i}{nFS\Gamma^*_{\mathrm{ox}} f} \tag{II.3.70}$$

The kinetic parameter κ is defined by Eq. (II.3.57).

Under chronoamperometric conditions (E = const.), the solution of Eq. (II.3.45) is

$$\Phi = \lambda\exp(-\alpha\varphi)\exp[-\lambda\exp(-\alpha\varphi)(1+\exp(\varphi))] \tag{II.3.71}$$

$$\Phi = it(nFS\Gamma^*_{\mathrm{ox}})^{-1} \tag{II.3.72}$$

$$\lambda = k_{\mathrm{s}}t \tag{II.3.73}$$

If $\varphi = 0$, Eq. (II.3.71) is reduced to

$$i/nFS\Gamma^*_{\mathrm{ox}} = k_{\mathrm{s}}\exp(-2k_{\mathrm{s}}t) \tag{II.3.74}$$

The maximum chronoamperometric response is defined by the first derivative of Eq. (II.3.71):

$$\partial\Phi/\partial\lambda = 0 \tag{II.3.75}$$

$$\lambda_{\max} = \exp(\alpha\varphi)[1+\exp(\varphi)]^{-1} \tag{II.3.76}$$

The second condition is:

$$\partial\lambda_{\max}/\partial\varphi = 0 \tag{II.3.77}$$

with the result:

$$\exp(\varphi_{\max}) = \frac{\alpha}{1-\alpha} \tag{II.3.78}$$

$$\lambda_{\max,\max} = \alpha^{\alpha}(1-\alpha)^{1-\alpha} \tag{II.3.79}$$

$$\Phi_{\max} = \frac{1-\alpha}{e} \tag{II.3.80}$$

This derivation shows that, for any electrode potential E, there is a certain dimensionless kinetic parameter $\lambda_{\max}$ which gives the highest response (Eq. II.3.76). The maximum of $\lambda_{\max}$ (Eq. II.3.79) is a parabolic function of the transfer coefficient: $0.5 \leq \lambda_{\max,\max} < 1$, for $0 < \alpha < 1$. If $\alpha = 0.5$, then $\lambda_{\max,\max} = 0.5$ and

$\Phi_{\max} = (2e)^{-1}$. This is in the agreement with Eq. (II.3.74). From the condition $\partial i/\partial k_s = 0$, it follows that $k_{s,\max} = (2t)^{-1}$ and $(i/nFS\Gamma^*_{ox})_{\max} = (2et)^{-1}$.

References

1. Autolab, Installation guide, EcoChemie BV, Utrecht, 1993; BAS 100A, Operation guide, Bioanalytical Systems, West Lafayette, 1987; Model 384 B, Operating manual, EG & G Princeton Applied Research, Princeton, 1983
2. Mirčeski V, Komorsky-Lovrić Š, Lovrić M (2007) Square-Wave Voltammetry. Springer, Berlin Heidelberg New York
3. de Souza D, Machado SAS, Avaca LA (2003) Quim Nova 26: 81
4. de Souza D, Codognoto L, Malagutti AR, Toledo RA, Pedrosa VA, Oliveira RTS, Mazo LH, Avaca LA, Machado SAS (2004) Quim Nova 27: 790
5. Osteryoung JG, Osteryoung RA (1985) Anal Chem 57: 101A
6. Osteryoung J, O'Dea JJ (1986) Square-wave voltammetry. In: Bard AJ (ed) Electro analytical chemistry, vol 14. Marcel Dekker, New York, p 209
7. Eccles GN (1991) Crit Rev Anal Chem 22: 345
8. Kalousek M (1948) Collect Czech Chem Commun 13: 105
9. Barker GC, Jenkins IL (1952) Analyst 77: 685
10. Barker GC (1958) Anal Chim Acta 18: 118
11. Ishibashi M, Fujinaga T (1952) Bull Chem Soc Jpn 25: 68
12. Kinard WF, Philp RH, Propst RC (1967) Anal Chem 39: 1557
13. Radej J, Ružić I, Konrad D, Branica M (1973) J Electroanal Chem 46: 261
14. Barker GC, Gardner AW, Williams MJ (1973) J Electroanal Chem 42: App. 21
15. Kalvoda R, Holub I (1973) Chem Listy 67: 302
16. Igolinski VA, Kotova NA (1973) Elektrokhimiya 9: 1878
17. Ramaley L, Krause MS Jr (1969) Anal Chem 41: 1362
18. Krause MS Jr, Ramaley L (1969) Anal Chem 41: 1365
19. Christie JH, Turner JA, Osteryoung RA (1977) Anal Chem 49: 1899
20. Ramaley L, Surette DP (1977) Chem Instrum 8: 181
21. Buchanan EB Jr, Sheleski WJ (1980) Talanta 27: 955
22. Yarnitzky C, Osteryoung RA, Osteryoung J (1980) Anal Chem 52: 1174
23. Anderson JA, Bond AM (1983) Anal Chem 55: 1934
24. Lavy-Feder A, Yarnitzky C (1984) Anal Chem 56: 678
25. Jayaweera P, Ramaley L (1986) Anal Instrum 15: 259
26. Wong KH, Osteryoung RA (1987) Electrochim Acta 32: 629
27. Ramaley L, Tan WT (1981) Can J Chem 59: 3326
28. Fatouros N, Simonin JP, Chevalet J, Reeves RM (1986) J Electroanal Chem 213: 1
29. Chen X, Pu G (1987) Anal Lett 20: 1511
30. Krulic D, Fatouros N, Chevalet J (1990) J Electroanal Chem 287: 215
31. Aoki K, Maeda K, Osteryoung J (1989) J Electroanal Chem 272: 17
32. Lovrić M (1995) Croat Chem Acta 68: 335
33. Krulic D, Fatouros N, El Belamachi MM (1995) J Electroanal Chem 385: 33
34. Molina A, Serna C, Camacho L (1995) J Electroanal Chem 394: 1
35. Brookes BA, Ball JC, Compton RG (1999) J Phys Chem B 103: 5289
36. Zachowski EJ, Wojciechowski M, Osteryoung J (1986) Anal Chim Acta 183: 47
37. Lovrić M (1994) Annali Chim 84: 379
38. O'Dea JJ, Osteryoung J, Osteryoung RA (1981) Anal Chem 53: 695
39. Elsner CI, Rebollo NL, Dgli WA, Marchiano SL, Plastino A, Arvia AJ (1994) ACH-Models Chem 131: 121
40. O'Dea JJ, Osteryoung J, Osteryoung RA (1983) J Phys Chem 87: 3911

41. O'Dea JJ, Osteryoung J, Lane T (1986) J Phys Chem 90: 2761
42. Go WS, O'Dea JJ, Osteryoung J (1988) J Electroanal Chem 255: 21
43. Ivaska AV, Smith DE (1985) Anal Chem 47: 1910
44. Nuwer MJ, O'Dea JJ, Osteryoung J (1991) Anal Chim Acta 251: 13
45. Fatouros N, Krulic D (1998) J Electroanal Chem 443: 262
46. O'Dea JJ, Wojciechowski M, Osteryoung J, Aoki K (1985) Anal Chem 57: 954
47. Whelan DP, O'Dea JJ, Osteryoung J, Aoki K (1986) J Electroanal Chem 202: 23
48. Aoki K, Tokuda K, Matsuda H, Osteryoung J (1986) J Electroanal Chem 207: 25
49. Ramaley L, Tan WT (1987) Can J Chem 65: 1025
50. Fatouros N, Krulic D, Lopez-Tenes M, El Belamachi MM (1996) J Electroanal Chem 405: 197
51. Komorsky-Lovrić Š, Lovrić M, Bond AM (1993) Electroanalysis 5: 29
52. Singleton ST, O'Dea JJ, Osteryoung J (1989) Anal Chem 61: 1211
53. Murphy MM, O'Dea JJ, Osteryoung J (1991) Anal Chem 63: 2743
54. Tallman DE (1994) Anal Chem 66: 557
55. Kounaves SP, O'Dea JJ, Chandrasekhar P, Osteryoung J (1986) Anal Chem 58: 3199
56. Wikiel K, Osteryoung J (1989) Anal Chem 61: 2086
57. Kumar V, Heineman W (1987) Anal Chem 59: 842
58. Kounaves SP, Deng W (1991) J Electroanal Chem 306: 111
59. Penczek M, Stojek Z (1986) J Electroanal Chem 213: 177
60. Kounaves SP, O'Dea JJ, Chandrasekhar P, Osteryoung J (1987) Anal Chem 59: 386
61. Wechter C, Osteryoung J (1989) Anal Chem 61: 2092
62. Aoki K, Osteryoung J (1988) J Electroanal Chem 240: 45
63. Brookes BA, Compton RG (1999) J Phys Chem B 103: 9020
64. Ball JC, Compton RG (1998) J Phys Chem B 102: 3967
65. Agra-Gutierrez C, Ball JC, Compton RG (1998) J Phys Chem B 102: 7028
66. Zeng J, Osteryoung RA (1986) Anal Chem 58: 2766
67. O'Dea JJ, Wikiel K, Osteryoung J (1990) J Phys Chem 94: 3628
68. Molina A (1998) J Electroanal Chem 443: 163
69. Fatouros N, Krulic D (1998) J Electroanal Chem 456: 211
70. Turner JA, Christie JH, Vuković M, Osteryoung RA (1977) Anal Chem 49: 1904
71. Barker GC, Gardner AW (1979) J Electroanal Chem 100: 641
72. Stefani S, Seeber R (1983) Annali Chim 73: 611
73. Zhang J, Guo SX, Bond AM, Honeychurch MJ, Oldham KB (2005) J Phys Chem B 109: 8935
74. Jadreško D, Lovrić M (2008) Electrochim Acta 53: 8045
75. Barker GC, Bolzan JA (1966) Z Anal Chem 216: 215
76. Ramaley L, Dalziel JA, Tan WT (1981) Can J Chem 59: 3334
77. Komorsky-Lovrić Š, Lovrić M, Branica M (1988) J Electroanal Chem 241: 329
78. Webber A, Shah M, Osteryoung J (1983) Anal Chim Acta 154: 105
79. Webber A, Shah M, Osteryoung J (1984) Anal Chim Acta 157: 1
80. Webber A, Osteryoung J (1984) Anal Chim Acta 157: 17
81. Komorsky-Lovrić Š (1987) J Electroanal Chem 219: 281
82. Komorsky-Lovrić Š, Lovrić M (1989) Fresenius Z Anal Chem 335: 289
83. Xu G, O'Dea JJ, Mahoney LA, Osteryoung JG (1994) Anal Chem 66: 808
84. Komorsky-Lovrić Š, Lovrić M, Branica M (1989) J Electroanal Chem 266: 185
85. Zelić M, Branica M (1991) J Electroanal Chem 309: 227
86. Zelić M, Branica M (1992) Electroanalysis 4: 623
87. Zelić M, Branica M (1992) Anal Chim Acta 262: 129
88. Lovrić M, Branica M (1987) J Electroanal Chem 226: 239
89. Lovrić M, Komorsky-Lovrić Š (1988) J Electroanal Chem 248: 239
90. Komorsky-Lovrić Š, Lovrić M, Branica M (1992) J Electroanal Chem 335: 297
91. O'Dea JJ, Osteryoung JG (1993) Anal Chem 65: 3090

92. Reeves JH, Song S, Bowden EF (1993) Anal Chem 65: 683
93. Komorsky-Lovrić Š, Lovrić M (1995) J Electroanal Chem 384: 115
94. Lovrić M (1991) Elektrokhimiya 27: 186
95. Komorsky-Lovrić Š, Lovrić M (1995) Anal Chim Acta 305: 248
96. Komorsky- Lovrić Š, Lovrić M (1995) Electrochim Acta 40: 1781
97. Komorsky-Lovrić Š (1996) Fresenius J Anal Chem 356: 306
98. Lovrić M, Mlakar M (1995) Electroanalysis 7: 1121
99. Mirčeski V, Lovrić M, Jordanoski B (1999) Electroanalysis 11: 660
100. Mirčeski V, Lovrić M (1999) Anal Chim Acta 386: 47
101. Komorsky-Lovrić Š (2000) J Electroanal Chem 482: 222
102. Mirčeski V, Lovrić M (1997) Electroanalysis 9: 1283
103. Garay F, Solis V, Lovrić M (1999) J Electroanal Chem 478: 17
104. O'Dea JJ, Osteryoung JG (1997) Anal Chem 69: 650
105. Lovrić M, Komorsky-Lovrić Š, Bond AM (1991) J Electroanal Chem 319: 1
106. Lovrić M, Pižeta I, Komorsky-Lovrić Š (1992) Electroanalysis 4: 327
107. Mirčeski V, Lovrić M (1999) Electroanalysis 11: 984
108. Mirčeski V, Lovrić M (1998) Electroanalysis 10: 976
109. Lovrić M, Komorsky-Lovrić Š, Murray RW (1988) Electrochim Acta 33: 739
110. O'Dea JJ, Ribes A, Osteryoung JG (1993) J Electroanal Chem 345: 287
111. Ostapczuk P, Valenta P, Nürnberg HW (1986) J Electroanal Chem 214: 51
112. Tercier M-L, Buffle J, Graziottin F (1998) Electroanalysis 10: 355
113. Zen J-M, Ting YS (1996) Anal Chim Acta 332: 59
114. Yarnitzky C, Smyth WF (1991) Int J Pharm 75: 161
115. Bobrowski A, Zarebski J (2000) Electroanalysis 12: 1177
116. Wang J, Tian B (1992) Anal Chem 64: 1706
117. Emons H, Baade A, Schoning MJ (2000) Electroanalysis 12: 1171
118. Petrovic SC, Dewald HD (1996) J Planar Chromatogr 9: 269
119. Hoekstra JC, Johnson DC (1999) Anal Chim Acta 390: 45
120. Galus Z (1994) Fundamentals of electrochemical analysis. Ellis Horwood, New York, Polish Scientific Publishers PWN, Warsaw
121. Nicholson RS, Olmstead ML (1972) Numerical solutions of integral equations. In: Matson JS, Mark HB, MacDonald HC (eds) Electrochemistry: calculations, simulations and instrumentation, vol 2. Marcel Dekker, New York, p 119